REDISCUSSION OF ECLIPSING BINARIES. PAPER XV. THE B-TYPE SUPERGIANT SYSTEM V1765 CYGNI

By John Southworth

Astrophysics Group, Keele University, Staffordshire, ST5 5BG, UK

V1765 Cyg is a detached eclipsing binary containing a B0.5 supergiant and a B1 main-sequence star, with an orbital period of 13.37 d and an eccentricity of 0.315. The system shows apsidal motion and the supergiant exhibits strong stochastic variability. V1765 Cyg was observed by the Transiting Exoplanet Survey Satellite over four sectors. We analyse these data to obtain the first determinate light curve model for the system. To this we add published spectroscopic orbits to infer masses of 23 ± 2 and 11.9 ± 0.7 $M_{\odot}$, and radii of 20.6 ± 0.8 and 6.2 ± 0.3 $R_{\odot}$. These properties are in good agreement with theoretical predictions for a solar chemical composition and an age around 7 Myr. We also present two epochs of blue-optical spectroscopy that confirm the luminosity classification of the primary star and appear to show absorption lines from the secondary star. Extensive spectroscopy and further analysis of the system is recommended.

Introduction

Detached eclipsing binaries (dEBs) are a vital source of empirical measurements of the properties of stars[1–3]. Such measurements typically show a good agreement with theoretical predictions except for stars of very low or very high mass. At lower masses, M-dwarfs are know to show a *radius discrepancy* which remains unsolved[4–6]. At higher masses, there is a *mass discrepancy* whereby stellar masses inferred from the stars' positions in the Hertzsprung-Russell diagram are systematically greater than those measured directly from orbital motion in binary systems[7]. Tkachenko et al.[8] have investigated this in detail using dEBs and concluded that it is stronger at lower surface gravities, and is partially caused by overestimation of the effective temperatures ($T_{\rm eff}$s) of massive stars from their optical spectra.

Massive stars are typically found in multiple systems[9,10] and most also show brightness variability due to a range of phenomena. Massive stars in dEBs have been found to show intrinsic variations due to stochastic low-frequency (SLF) variability[11,12] and β Cephei pulsations[13–15]. At lower masses, A- and F-stars in dEBs can show variability due to δ Scuti[16–19] and γ Doradus pulsations[20–22]. In all cases the pulsations can be perturbed or excited by tidal effects in close binary systems[23,24,18,22].

In this work we present the first analysis of extensive space-based photometry for the bright B-type supergiant system V1765 Cyg, which has a long observational history. The new photometric data also exhibit a strong signature of SLF

Table I: *Basic information on V1765 Cyg.*

Property	*Value*	*Reference*
Right ascension (J2000)	19:48:50.60	[27]
Declination (J2000)	+33:26:14.2	[27]
Bright Star Catalogue	HR 7551	[28]
Henry Draper designation	HD 187459	[29]
Gaia DR3 designation	2034968875123889536	[27]
Gaia DR3 parallax	0.6895 ± 0.0250 mas	[27]
TESS Input Catalog designation	TIC 59632148	[30]
B magnitude	6.578 ± 0.014	[31]
V magnitude	6.463 ± 0.010	[31]
J magnitude	6.027 ± 0.019	[32]
H magnitude	6.034 ± 0.018	[32]
K_s magnitude	6.030 ± 0.020	[32]
Spectral type	B0.5 Ib + B1 V	[33], This work

variability. See ref.[25] for a detailed description of our project and ref.[26] for a review of the impact of space-based photometry on binary star science.

V1765 Cygni

V1765 Cyg was announced as a spectroscopic binary by Plaskett & Pearce[34]. The primary component (hereafter star A) is a B0.5 supergiant and is the source of the observed SLF variability. The secondary component (star B) is of similar $T_{\rm eff}$ but is much smaller than the supergiant component. For clarity, star A is eclipsed (i.e. is at superior conjunction) by star B at primary eclipse.

Mayer & Chochol[35] discovered the eclipses and also commented on the presence of "irregular fluctuations in the range of about 0.06 mag". They also obtained RVs of star A and asserted the presence of apsidal motion. However, they did not attempt a solution of the light curve. Percy & Welch[36] confirmed the presence of "pronounced intrinsic variability".

The spectral type of the much brighter component of the system has been given as either B0.5 Ib[33,37,38] or B0.5 II[39,40]. A classification of B0.5 Ib + B2 V was given by Hill & Fisher[41] (hereafter HF84).

HF84 presented the most detailed analysis of the system thus far, based on photographic spectra subsequently converted to electronic format for analysis. They found star B to show up reasonably well in He I lines and determined RVs via cross-correlation. The plotted cross-correlation functions (HF84's fig. 1) show that the two components are never resolved, so the RVs were obtained by fitting double overlapping Gaussian functions. Apsidal motion was detected but at a level below that required for confirmation. HF84 presented mass and radius estimates for both components but relied on a calibration of radius versus spectral type for star A as the solution of the light curves from Mayer & Chochol[35] was indeterminate.

Mayer et al.[42] obtained new photometry and spectroscopy and estimated the masses and radii of the components, giving values similar to those found by

HF84. However, they preferred an earlier spectral type for star B of of B1 V or even B0 V. Raja[43] presented further photographic spectroscopy in which they were not able to find a sign of star B, but found an apsidal motion of 7.3×10^{-4} deg d^{-1}, in agreement with previous results.

Popper[44] presented a small number of high-quality spectra of V1765 Cyg. He obtained a much larger rotational velocity of $\sim$200 km s^{-1} for star A, versus the value of 135 ± 10 km s^{-1} measured by HF84. He was also not able to find clear evidence of spectral lines of star B despite being sensitive to much smaller lines than expected based on the light ratio of the system inferred by HF84. He concluded that the system was unfavourable for further analysis due to the difficulties it poses for both spectroscopy and photometry.

Percy & Khaja[45] presented further photometry of the system from which they measured the eclipse depths and found a possible slow increase in brightness. Since then, V1765 Cyg has mostly been left well alone save for appearances in large sky surveys. The MASCARA cameras[46] have observed V1765 Cyg extensively and obtained 12 057 photometry measurements of the system[47] which show the eclipses and intrinsic variability.

In the current work we use extensive new light curves to investigate the photometric properties of the system, infer its physical properties, examine two new spectra, and draw attention to the similarity between V1765 Cyg and V380 Cyg. We conclude with a discussion on the future prospects for analysis of this important but challenging binary system.

Photometric observations

V1765 Cyg has been observed four times by the NASA Transiting Exoplanet Survey Satellite[48] (TESS). The data from sector 14 (2019/07/18 to 2019/08/15) were obtained at a cadence of 1800 s, and the data from sector 41 (2021/07/23 to 2021/08/23) and sectors 54 and 55 (2022/07/09 to 2022/09/01) had an observing cadence of 600 s. We used the LIGHTKURVE package[49] to download the data and reject points flagged as bad. We adopted the simple aperture photometry (SAP) data[50] for consistency with previous papers in this series.

We converted the data to differential magnitude and subtracted the median magnitude for further analysis. The numbers of datapoints are 1237, 3505, 3571 and 3645, for sectors 14, 41, 54 and 55, respectively. Data with a 120 s cadence are available for all but the first sector, but were not used in our analysis because the system does not vary on a timescale fast enough to require the higher sampling rate.

The data are shown in Fig. 1. The light curves clearly show the existence of annular primary eclipses, total secondary eclipses, orbital eccentricity and SLF variability.

Spectroscopic observations

We obtained spectroscopy of V1765 Cyg on the nights of 2023/07/02 and 2023/07/04 in order to investigate the suitability of the system for detailed

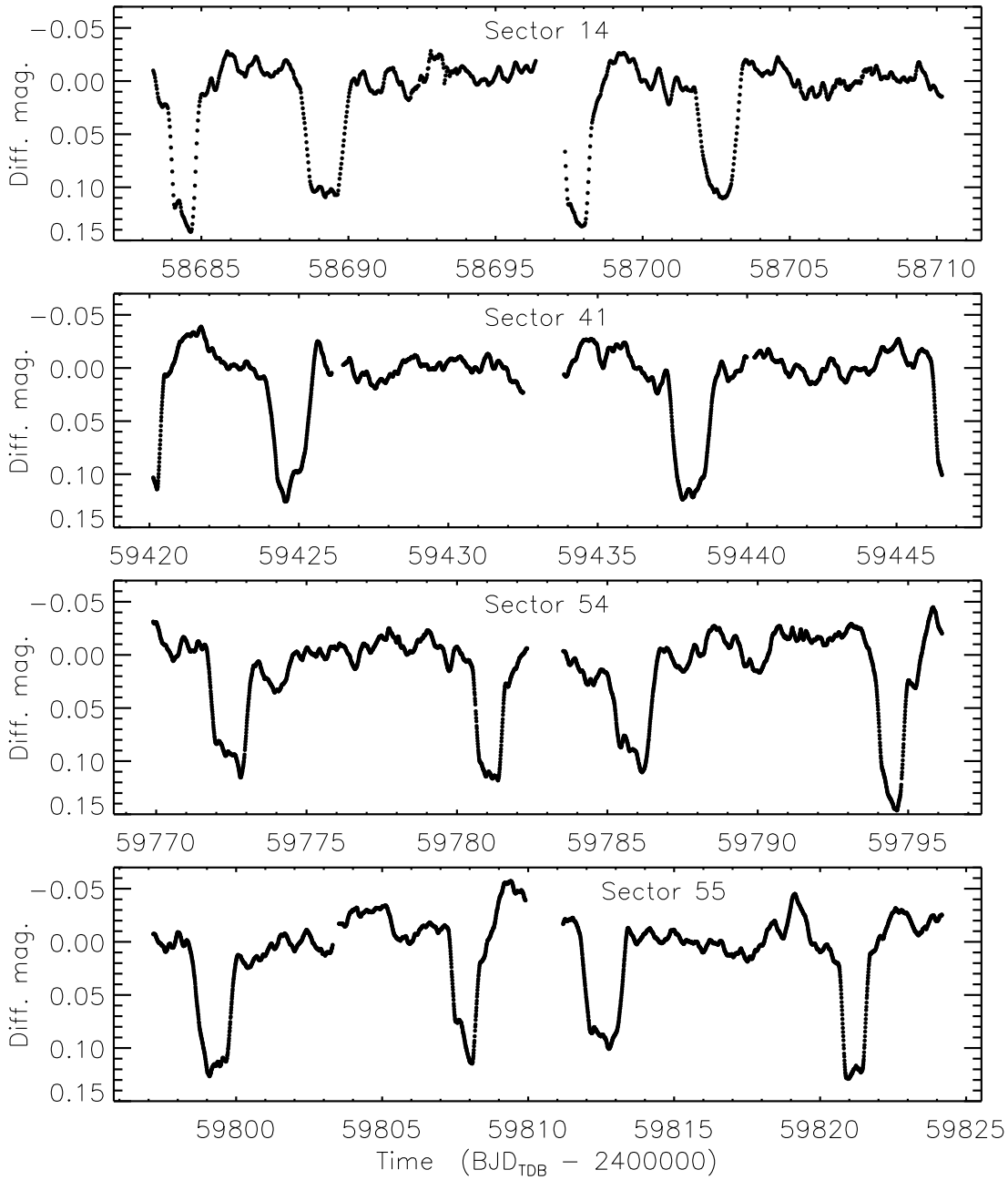

FIG. 1: TESS short-cadence SAP photometry of V1765 Cyg. The flux measurements have been converted to magnitude units then rectified to zero magnitude by subtraction of the median. The individual sectors are labelled.

analysis. Our observing run lasted 7 nights and covered only half of the orbit of V1765 Cyg, so we made no attempt to obtain sufficient data for measuring the spectroscopic orbits of the stars. Instead we obtained two spectra on the first night at a time when the two stars had approximately the same RV, and three spectra on the second night when the stars were close to their largest RV separation.

We used the Isaac Newton Telescope (INT), Intermediate Dispersion Spectrograph (IDS) with the 235 mm camera, the EEV10 CCD, the H2400B grating, a

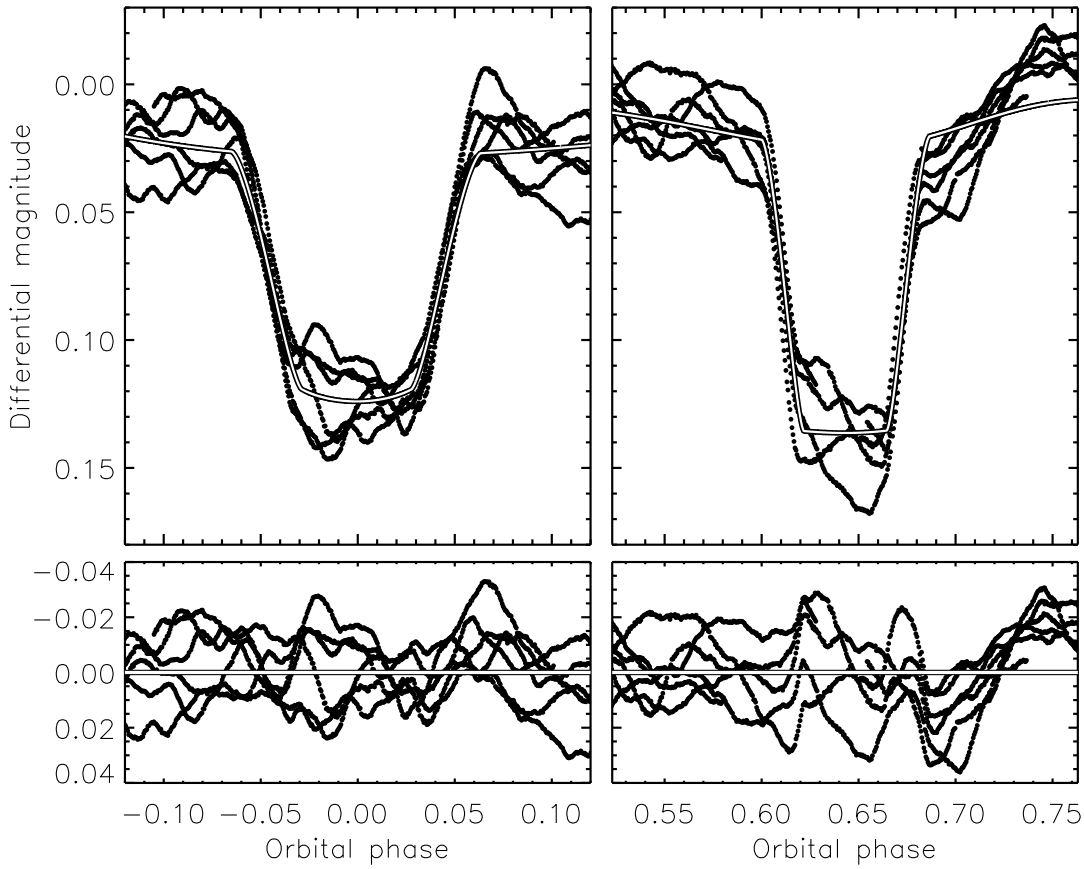

FIG. 2: The TESS light curves of V1765 Cyg from sectors 41, 54 and 55, with 600 s cadence (filled circles) versus the best fit from JKTEBOP (white-on-black line) as a function of orbital phase. The primary eclipse is shown on the left and the secondary eclipse on the right. The residuals are shown on an enlarged scale in the lower panel.

central wavelength of 420 nm, and a 1″ slit. This gave spectra with a reciprocal dispersion of 0.24 Å mm^{-1}, a resolution of 0.5 Å as measured from the Cu+Ar lamps used for wavelength calibration, and a spectral coverage of 410–465 nm. The data were reduced using a pipeline currently under construction (see ref.[51]).

The spectra from each night were taken at the same time so were summed to give two overall spectra. The total exposure time was 240 s on the first night and 720 s on the second night, with the latter being significantly longer to compensate for the presence of moderate cloud.

Light curve analysis

We modelled the light curve of V1765 Cyg from TESS using version 43 of the JKTEBOP* code[52,53]. Star A is formally too deformed to be suitable for JKTEBOP, but the intrinsic variability of the system is much more important than the expected bias in the parameters and we were keen to utilise the error estimation algorithms available in the code. We analysed the data with a cadence of 600 s from sectors 41, 54 and 55 simultaneously. Sector 14 was not used due

*http://www.astro.keele.ac.uk/jkt/codes/jktebop.html

Table II: *Adopted parameters of V1765 Cyg measured from the TESS light curves using the* JKTEBOP *code. The uncertainties are 1σ and were determined using residual-permutation simulations.*

Parameter	*Value*
Fitted parameters:	
Time of primary eclipse ($\mathrm{BJD_{TDB}}$)	2459438.122 ± 0.021
Orbital period (d)	13.37441 ± 0.00075
Orbital inclination (°)	84.3 ± 1.0
Sum of the fractional radii	0.344 ± 0.011
Ratio of the radii	0.3006 ± 0.0090
Central surface brightness ratio	1.30 ± 0.13
$e \cos \omega$	0.2211 ± 0.0027
$e \sin \omega$	-0.217 ± 0.021
Derived parameters:	
Fractional radius of star A	0.2643 ± 0.0074
Fractional radius of star B	0.0794 ± 0.0038
Light ratio $\ell_\mathrm{B}/\ell_\mathrm{A}$	0.117 ± 0.010
Orbital eccentricity	0.310 ± 0.014
Argument of periastron (°)	315.5 ± 2.9

to the lower sampling rate. Conversely, the data with a higher cadence of 120 s available in the last three sectors were not used because it greatly oversamples the changes in brightness due to both eclipses and pulsations.

We fitted for the sum ($r_\mathrm{A} + r_\mathrm{B}$) and ratio ($k = r_\mathrm{B}/r_\mathrm{A}$) of the fractional radii of the stars (r_A and r_B), and their central surface brightness ratio in the TESS passband (J). We fitted for the orbital period (P), reference time of primary minimum (T_0), and the eccentricity (e) and argument of periastron (ω) in terms of their Poincaré elements ($e \cos \omega$ and $e \sin \omega$). A set of straight lines versus time were included for the baseline brightness of the system, one for each half-sector of TESS data, and the coefficients of the lines were included as fitted parameters. We included limb darkening using the simple linear law[54] with the coefficients of both stars fixed to 0.2. More sophisticated laws are not justified due to the strong SLF variability in the light curve, and attempts to fit for the coefficients were unsuccessful for the same reason. We also found that third light was not estimable from the data, so fixed it at zero.

The first result of the analysis above is that the secondary eclipse is deeper than the primary. This conflicts with the standard definition of which is primary and which is secondary, but we have chosen to retain our labelling of the stars so the dominant component remains star A. From this it can be deduced that star B has a higher surface brightness, and thus T_eff, than the supergiant star A. Our results are otherwise very much as expected, and are given in Table II. The values of e and ω agree well with previous spectroscopic results.

For the record, we were able to obtain an almost identical fit for the inverse of k (i.e. 3.0 versus 0.3). We rejected this solution as being inconsistent with the the model of the system developed by HF84.

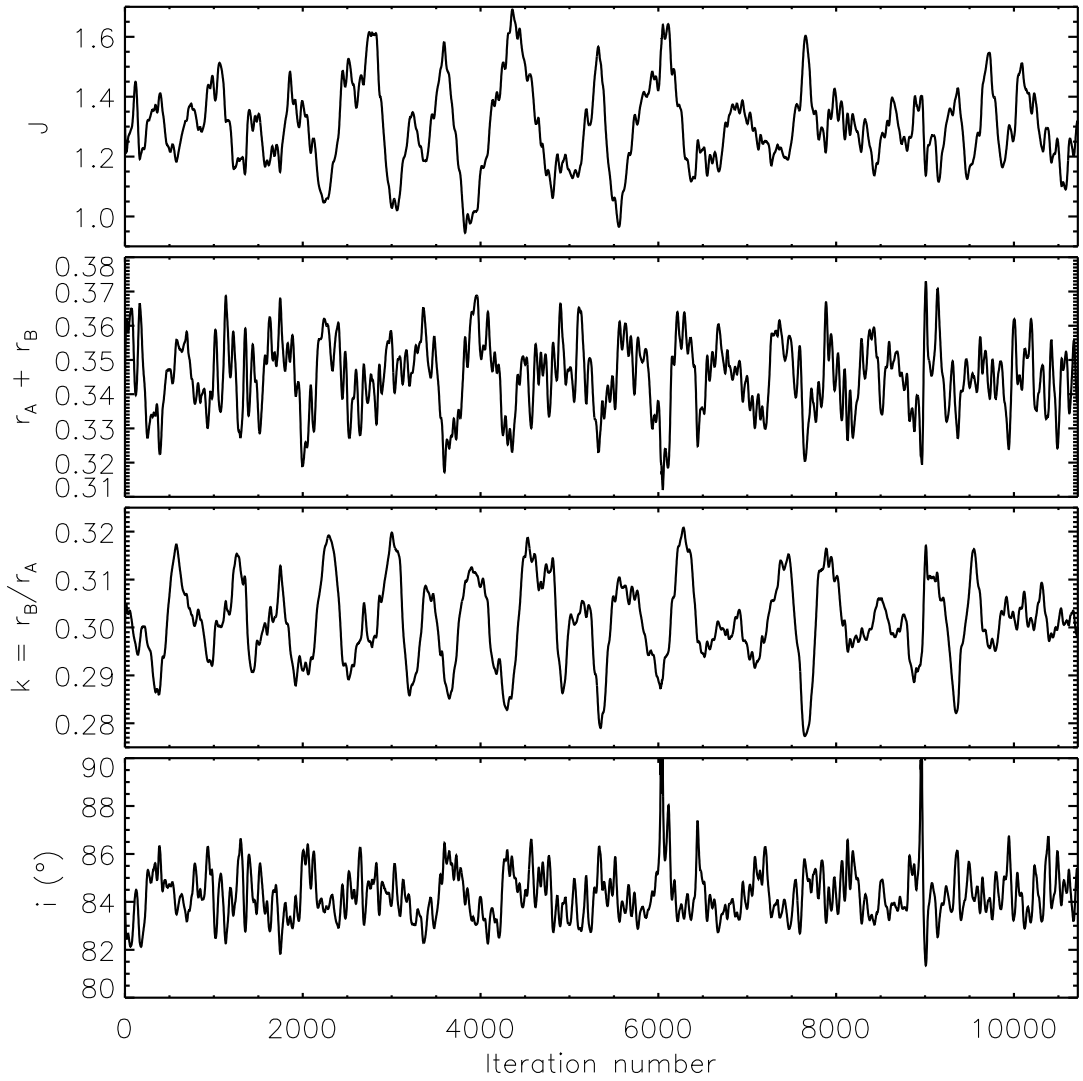

FIG. 3: Variation in the best-fitting values of four of the photometric parameters during the RP simulations, as the residuals are cyclically shifted through the light curve.

Light curve uncertainties

The light curve is dominated by the SLF variability, which is essentially red noise from the point of view of eclipse modelling. We therefore used only residual-permutation (RP) simulations[55] to determine the uncertainties in the fitted parameters. These results are also given in Table II. Although the data in hand fully cover six orbits of the system, the strong deformation of the eclipses by the SLF signature complicates any attempts to model them. Our errorbars account for this but may still be underestimates.

To further illustrate the effect of the SLF variations on the parameters measured from the eclipses, in Fig. 3 we plot the variation of the best-fitting values of four selected parameters through the RP simulation run. The residuals versus the best JKTEBOP fit are shifted by one datapoint between each successive iteration, and the gradual progression of red noise through the light curve causes

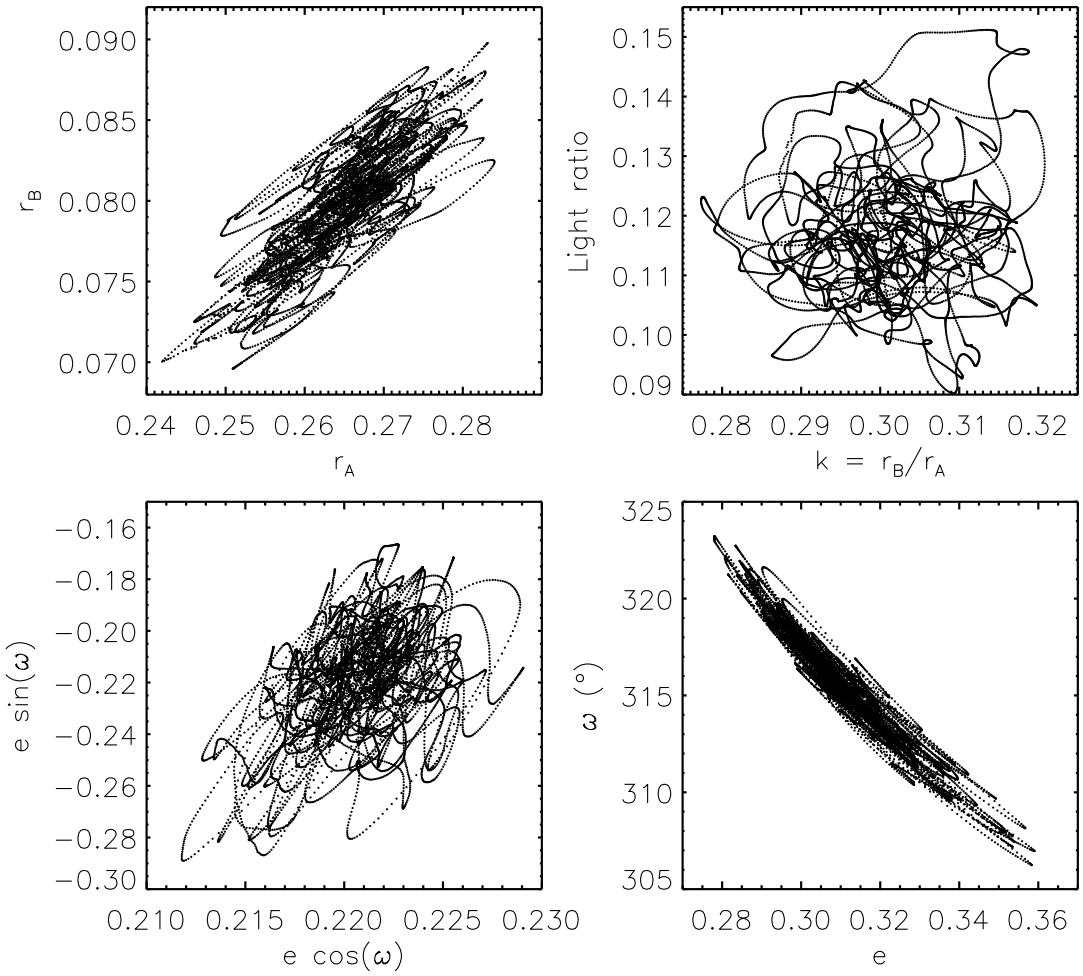

FIG. 4: Comparison plots for the best-fitting values of pairs of parameters during the RP simulations.

systematic changes in the fitted parameter values. The most-affected parameter is J, which depends primarily on the relative depths of the primary and secondary eclipses. The eclipse depths are significantly changed by the SLF noise, causing a large uncertainty in J and thus the ratios of the $T_{\rm eff}$s of the two stars. A similar signature is seen in the ratio of their radii. The variation for $r_{\rm A} + r_{\rm B}$ and i is much faster: these parameters depend on the shapes and durations of the ascending and descending branches of the eclipses, which in turn are shorter than the total eclipse durations. The properties of V1765 Cyg mean it allows a beautiful demonstration of these effects.

Fig. 4 shows the variations between pairs of parameters over the RP simulations. The first panel shows $r_{\rm B}$ versus $r_{\rm A}$ and a clear correlation can be seen. The second panel shows the light ratio versus the radius ratio: it has a satisfying child's-scribble appearance but the correlation is small. The inference from this panel is that a spectroscopic light ratio would not be useful in improving the precision of the radius measurements. The remaining two panels show the orbital shape parameters in two forms: the poor determinacy of $e \sin \omega$ (which depends on the ratio of the eclipse durations) is obvious. The much greater cor-

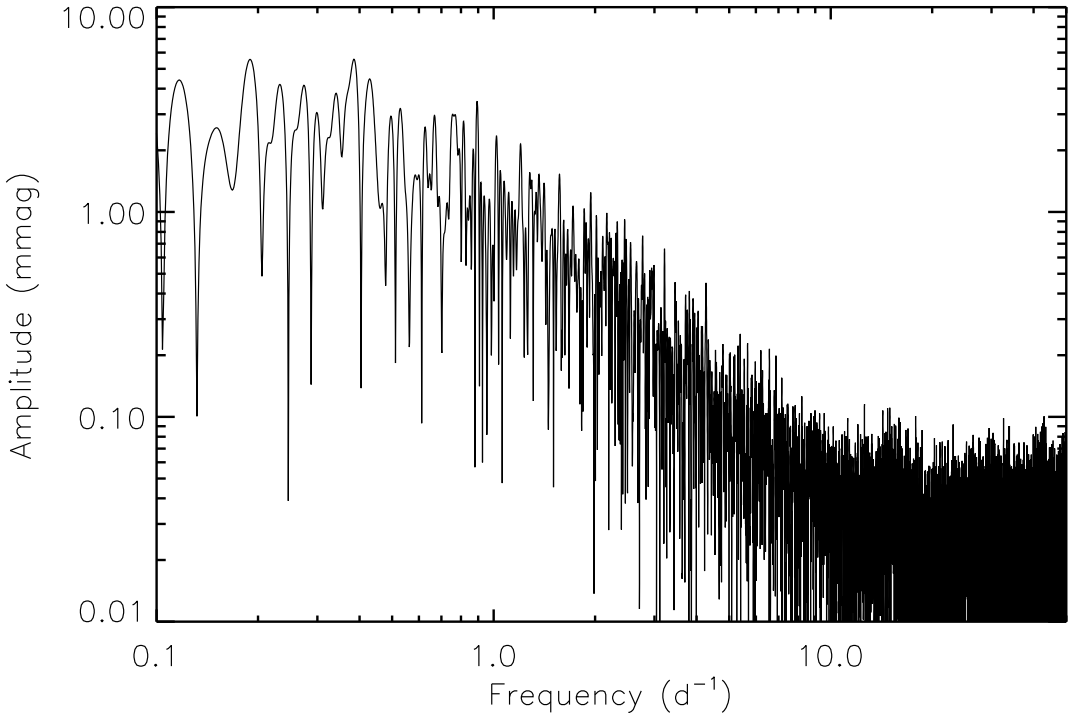

FIG. 5: Periodogram of the residuals of the best fit for TESS sectors 54 and 55, calculated using the PERIOD04 code.

relation between e and ω, versus $e\cos\omega$ and $e\sin\omega$, is also clear: this reiterates the advantage of fitting for the Poincaré elements rather than e and ω directly.

Stochastic low-frequency variability

The intrinsic variability in the light curves of V1765 Cyg is obvious and can safely be assumed to arise from the supergiant star A. To investigate it further we used the best fit from JKTEBOP found above, restricted it to sectors 54 and 55 as these data are semi-continuous, selected the residuals of the best fit, and calculated a periodogram using the PERIOD04 code[56]. The result is shown in Fig. 5. A periodogram of the 120 s cadence data from sector 55 shows no significant signal at higher frequencies, up to the Nyquist limit for these data of 350 d^{-1}.

Fig. 5 shows excess power at frequencies below 5 d^{-1} with a large number of peaks with significant amplitude. This is characteristic of SLF variability[11,57], has been seen before in dEBs[58,12], and is attributable to internal gravity waves excited at the boundary of a convective region within the star[59,60]. The two highest peaks occur at 0.19 and 0.38 d^{-1} and have amplitudes of 5.6 mmag.

Spectroscopic properties

V1765 Cyg is spectroscopically difficult due to the large line broadening and SLF-induced line profile variability of star A. HF84 identified faint peaks in the cross-correlation functions arising from star B which was found to be ap-

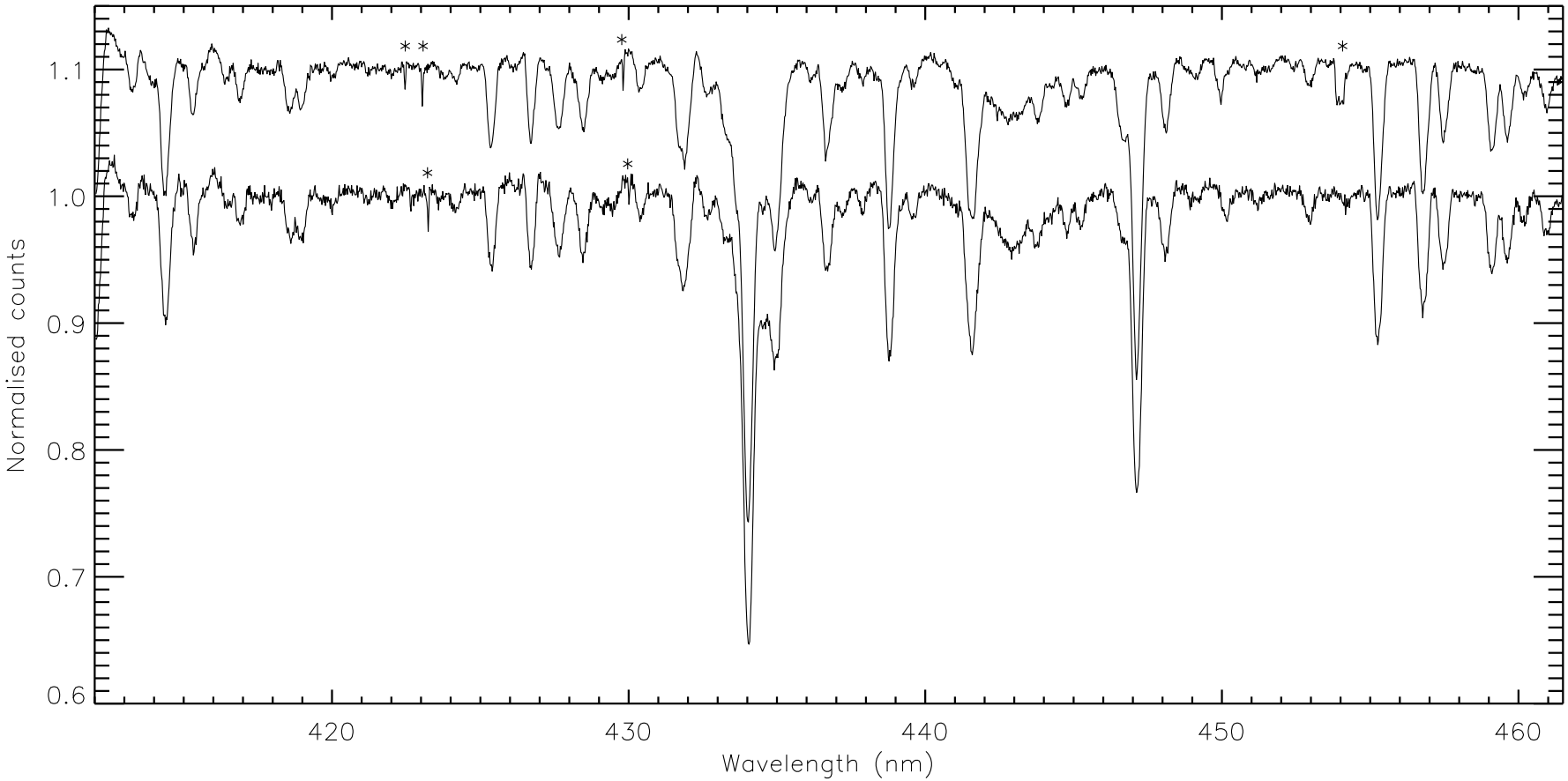

FIG. 6: The two combined spectra of V1765 Cyg taken when the RVs of the two stars were the same (normalised to 1.0) and when they show their greatest separation (offset by +0.1). The second spectrum has been shifted by −0.2 nm to align the spectral lines of star A. CCD cosmetics are indicated with asterisks.

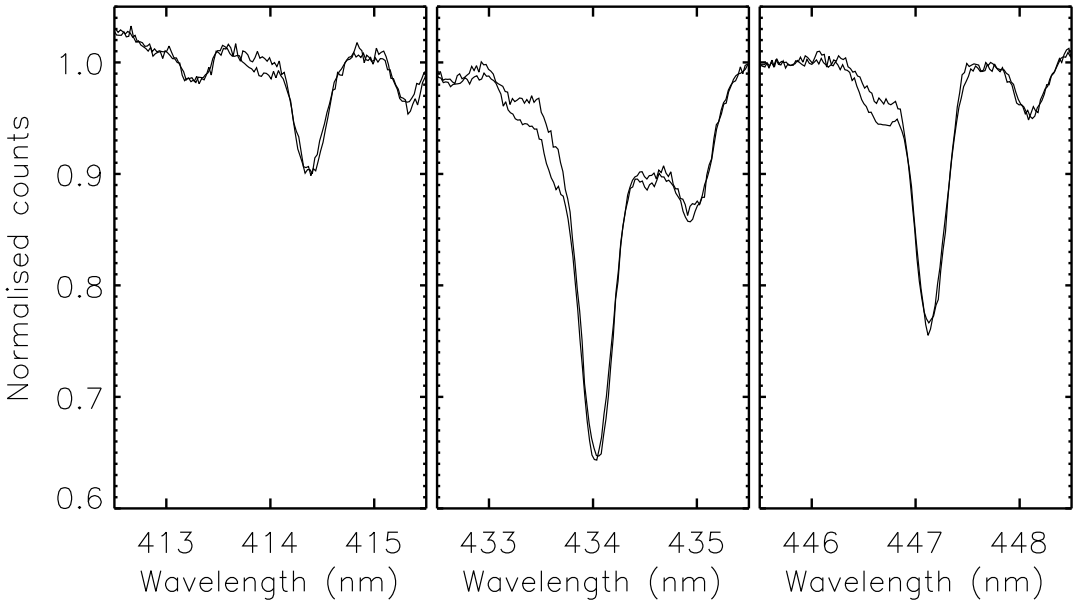

FIG. 7: Comparison between the two combined spectra of V1765 Cyg in the region of the He I 4143 Å, Hγ 4340 Å and He I 4471 Å lines. The two spectra were aligned in wavelength to make the strong lines from star A overlap.

proximately ten times fainter than star A at blue-optical wavelengths. This was questioned by Popper[44], who was not able to confidently identify lines of star B despite having spectra of much better quality. A relevant point here is that the light ratio we found from the TESS light curve matches that inferred by HF84 from the relative areas of the cross-correlation function peaks.

As described above, we obtained two INT/IDS spectra in order to investigate this further. These are shown in Fig. 6, where the spectrum from the second night has been offset by +0.1 from that for the first night, and also shifted by −0.20 nm to remove the RV variation of star A relative to the first spectrum. The first spectrum was taken at orbital phase 0.617 – at the beginning of totality during secondary eclipse – so contains light from star A only. The second spectrum was taken at phase 0.768 so includes light from both stars, with a velocity separation of 376 km s^{-1}.

In both cases the spectra are corrected for the barycentric velocity. The spectra show strong H, He and O absorption, plus C, N, Si and Mg lines and a diffuse interstellar band centred at ∼443 nm. The strong O II lines at 4348 and 4416 Å confirm the supergiant classification, and are strong enough to support a luminosity class of 1a rather than the typically-quoted 1b.

A careful comparison of the two spectra reveals the appearance of three faint absorption lines to the left of the main lines on the second night (see Fig. 7). These are exactly where we would expect to find lines from star B, and similar features are *not* seen where they should not be (e.g. for the O II lines). This suggests that V1765 Cyg may well be double-lined and thus suitable for direct measurement of its masses and radii. This work will be helped by obtaining extensive new high-quality spectroscopy and analysing them using methods not available to previous workers such as two-dimensional cross-correlation[61],

Table III: *Plausible physical properties of V1765 Cyg defined using the nominal solar units given by IAU 2015 Resolution B3 (ref.[68]).*

Parameter	*Star A*	*Star B*
Mass ratio $M_{\rm B}/M_{\rm A}$	0.50 ± 0.02	
Semimajor axis of relative orbit ($\mathcal{R}^{\rm N}_\odot$)	78 ± 2	
Mass ($\mathcal{M}^{\rm N}_\odot$)	23 ± 2	11.9 ± 0.7
Radius ($\mathcal{R}^{\rm N}_\odot$)	20.6 ± 0.8	6.2 ± 0.3
Surface gravity (log[cgs])	3.19 ± 0.03	3.93 ± 0.04
Effective temperature (K)	25000 ± 2000	26500 ± 2500
Luminosity $\log(L/\mathcal{L}^{\rm N}_\odot)$	5.18 ± 0.14	4.23 ± 0.17
$M_{\rm bol}$ (mag)	-8.2 ± 0.4	-5.8 ± 0.4
Distance (pc)	1520 ± 110	

broadening functions[62] and spectral disentangling[63]. The last method is most promising (e.g. ref.[64]) but may be affected by the line-profile variations from the stochastic variability. We defer further analysis until suitable spectra are available.

Physical properties of V1765 Cyg

This work presents the first determinate solution of the light curve of V1765 Cyg and thus enables a more direct estimation of the properties of the system. For this the velocity amplitudes of the stars' spectroscopic orbits are needed. There is only one source available in the literature, HF84, and their results were questioned by Popper[44]. We chose to adopt (approximately) the values from HF84 but with increased errorbars to account for the conflicting results: $K_{\rm A} = 103 \pm 2$ km s^{-1} and $K_{\rm B} = 206 \pm 10$ km s^{-1}.

HF84 adopted a $T_{\rm eff}$ of 25 000 K for star A from a calibration versus spectral type by Underhill et al.[65], to which we add a plausible errorbar of 2000 K. The surface brightness ratio from the light curve analysis (Table II) then gives a $T_{\rm eff}$ of 26500 ± 2500 K for star B, which implies a spectral type of B1 V using the calibration of Pecaut & Mamajek[66]. Wu et al.[67] gave a higher $T_{\rm eff}$ of 26556 ± 1934 K for the system (analysed as if it were a single star) but we did not use this value as it yielded a distance to the system significantly longer than that from the *Gaia* parallax (see below). More precise and accurate $T_{\rm eff}$ values could be obtained from spectroscopy of the system in future.

Armed with these numbers, we calculated the expected physical properties of V1765 Cyg using using the JKTABSDIM code[69] in our usual way for this series of papers. However, in this case, the numbers should not be taken as definitive due to the disagreement over whether the RVs of star B are reliable. The inferred properties are given in Table III.

To determine the distance to the system we used the Tycho-2 B and V magnitudes[31] which are averages of 14 measurements each, the 2MASS JHK_s magnitudes[32] which are single measurements taken at orbital phase 0.78 (i.e. outside eclipse), and bolometric corrections from Girardi et al.[70]. An interstellar reddening of $E(B-V) = 0.43 \pm 0.10$ mag is needed to bring the BV and JHK_s

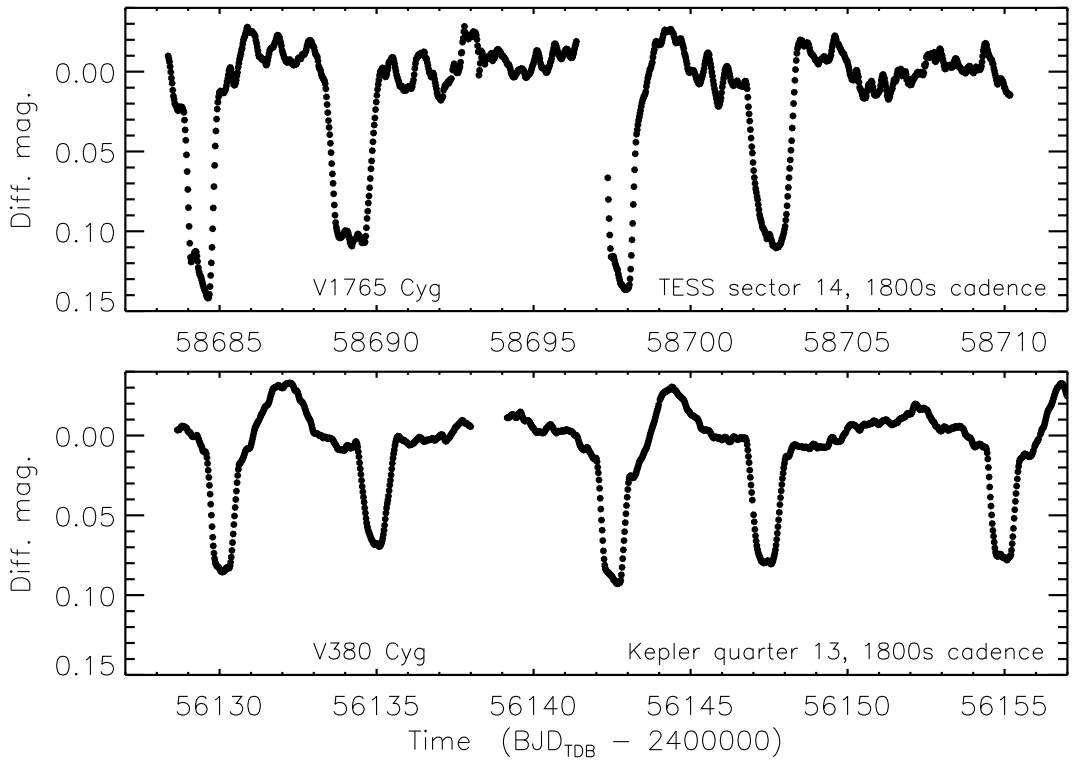

FIG. 8: Comparison between the TESS light curve of V1765 Cyg (top) and the *Kepler* light curve of V380 Cyg (bottom). The y-axes are the same, and the x-axes are of the same duration, in the two panels.

distances into agreement, giving a final K-band distance of 1520 ± 110 pc which is concordant with the distance of 1450 ± 53 pc from the *Gaia* DR3 parallax. This agreement supports the reliability of the approximate system parameters put forward in Table III.

The similarity of V1765 Cyg and V380 Cyg

One object stands out as being rather similar to V1765 Cyg. V380 Cyg is a dEB containing B1 III and B2 V components with an orbital period of 12.4 d, an eccentricity of 0.222, and an extensive observational history[71–73,64,74,58].

In Fig. 8 we show light curves of the two systems with the same axis scales. We chose TESS sector 14 for V1765 Cyg and *Kepler*[75] quarter 13 for V380 Cyg, in both cases with a sampling rate of 1800 s. It can be seen that the eclipses are slightly deeper and longer in V1765 Cyg, and in particular the SLF variability is much stronger. Although the more evolved components in the two systems have almost the same fractional radii, V380 Cyg has a much more pronounced "orbital hump" at periastron passage shortly after primary eclipse.

Tkachenko et al.[58] found these masses and radii for the components of V380 Cyg: $M_{\rm A} = 11.43 \pm 0.19$ M$_\odot$, $R_{\rm A} = 15.71 \pm 0.13$ R$_\odot$, $M_{\rm B} = 7.00 \pm 0.14$ M$_\odot$ and $R_{\rm B} = 3.82 \pm 0.05$ R$_\odot$. V1765 Cyg is therefore a more extreme version of V380 Cyg. Tkachenko et al. used 406 spectra in their investigation – V1765 Cyg would likely need a similar amount because the larger light ratio (so star B is relatively

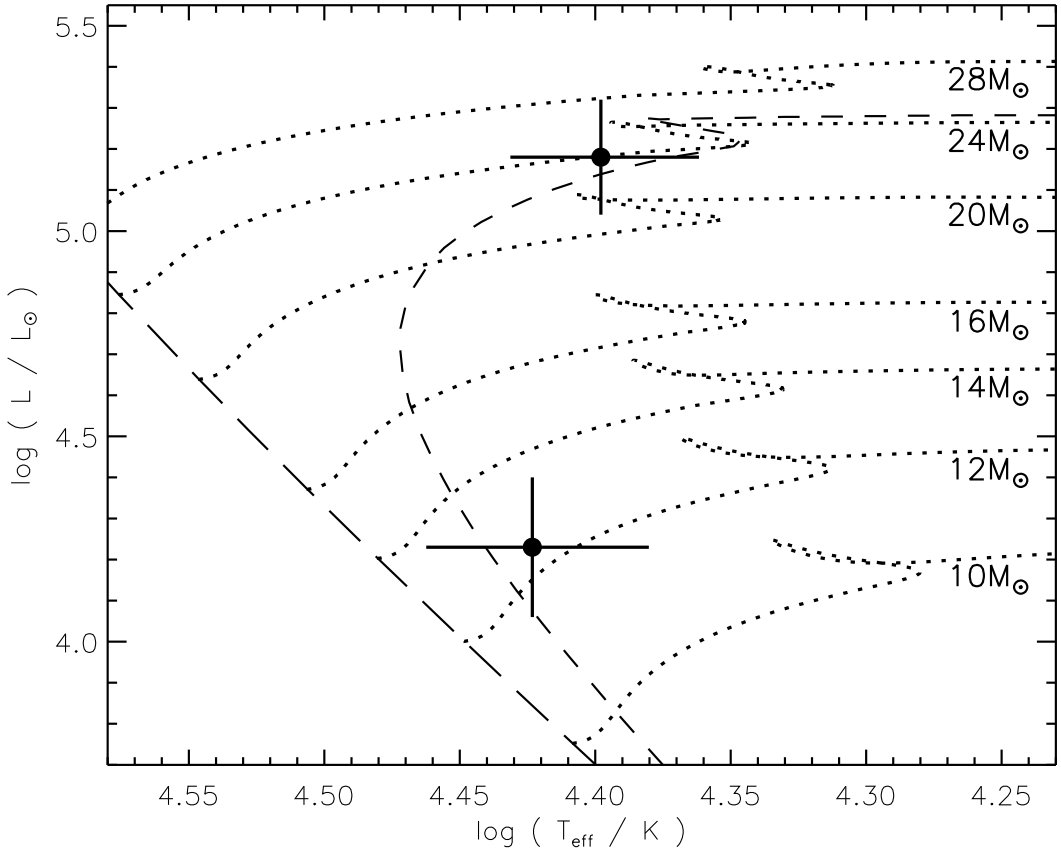

FIG. 9: Hertzsprung-Russell diagram for the components of V1765 Cyg (filled circles with errorbars) and the predictions of the PARSEC 1.2S models[76] for selected masses (dotted lines with masses labelled). The zero-age main sequence is indicated with a long-dashed line, and a 7-Myr isochrone with a short-dashed line.

brighter) will be offset by the stronger variability of star A. Whilst this is a *lot* of spectra, the brightness of the system means such a number is achievable.

Comparison with theoretical models

Although the properties in Table III are not definitive, a brief check against theoretical predictions could be illuminating. For this we adopted the PARSEC 1.2S models from Chen et al.[76]. A reasonable agreement is found in plots of mass versus radius and $T_{\rm eff}$ (not shown) for a metal abundance of $Z = 0.02$ and an age of 7 ± 1 Myr. This supports the lower of the two $T_{\rm eff}$ measurements discussed above. The radius of star B is approximately 3σ larger than predicted, but the two $T_{\rm eff}$ values sit perfectly on the predictions.

Fig. 9 shows a Hertzsprung-Russell diagram with the components of V1765 Cyg and predictions from the PARSEC models for a range of masses. The figure includes the zero-age main sequence and an isochrone for an age of 7 Myr. The agreement between observation and theory is good. More precise properties of V1765 Cyg are needed to provide a useful test of the models.

Summary and conclusions

V1765 Cyg is a very interesting totally-eclipsing binary containing a B0.5 supergiant and a B1 main-sequence star on a 13.37 d orbit with an eccentricity of 0.315. Extensive previous work has yielded a reliable spectroscopic orbit for star A and a less reliable one for star B. Whilst the reality of the detection of star B in the spectra has been questioned, the resulting RVs lead us to a plausible set of properties for the system.

In this work we analysed four sectors of observations from the TESS mission, allowing us to determine the radii of the stars from the eclipse profiles. Previous radius estimates were based only on calibrations versus spectral type. We arrive at physical properties in agreement with published values but on a more solid empirical basis. These properties can be matched by the PARSEC models for a solar chemical composition and an age in the region of 7 Myr.

Star A shows strong stochastic brightness variations of the SLF type, which distort the eclipse shapes and complicate both photometric and spectroscopic analyses. More extensive photometry, should the opportunity arise, may allow specific pulsation modes to be identified. V1765 Cyg is similar to but a more extreme version of the well-studied V380 Cyg system.

Apsidal motion has been detected in this system[43,43], although the detection has been questioned (HF84). The value of ω we deduced from the light curve supports the existence of apsidal motion, as it is significantly greater than the values found in the old spectroscopic studies. A more detailed analysis of this phenomenon would be rewarding.

We also presented two epochs of medium-resolution spectroscopy which confirm the spectral classification of star A. Star B produces approximately 10% of the light of the system and our spectra show evidence of its absorption lines which encourages further study. We strongly recommend that a large set of high-quality spectra are obtained for this system to confirm the detection of star B and for measurement of the atmospheric parameters and spectroscopic orbits of both stars. Such work will be difficult, but will be helped by the development of new analysis tools since the last detailed spectroscopic study of this system. The nature of the V1765 Cyg system makes such work well worth pursuing.

Acknowledgements

I am grateful to Steve Overall for assistance in obtaining the INT spectra, where by "assistance" I mean he actually performed the observations whilst I sat there, watched, and drank tea. This paper includes data collected by the TESS mission and obtained from the MAST data archive at the Space Telescope Science Institute (STScI). Funding for the TESS mission is provided by the NASA's Science Mission Directorate. STScI is operated by the Association of Universities for Research in Astronomy, Inc., under NASA contract NAS 5–26555. The following resources were used in the course of this work: the NASA Astrophysics Data System; the SIMBAD database operated at CDS, Strasbourg, France; and the arχiv scientific paper preprint service operated by Cornell University.

References

1 J. Andersen, *A&ARv*, **3**, 91, 1991.
2 G. Torres, J. Andersen & A. Giménez, *A&ARv*, **18**, 67, 2010.
3 J. Southworth, in *Living Together: Planets, Host Stars and Binaries* (S. M. Rucinski, G. Torres & M. Zejda, eds.), 2015, *Astronomical Society of the Pacific Conference Series*, vol. 496, p. 321.
4 D. T. Hoxie, *A&A*, **26**, 437, 1973.
5 C. H. Lacy, *ApJS*, **34**, 479, 1977.
6 G. Torres, *Astronomische Nachrichten*, **334**, 4, 2013.
7 A. Herrero *et al.*, *A&A*, **261**, 209, 1992.
8 A. Tkachenko *et al.*, *A&A*, **637**, A60, 2020.
9 H. Sana *et al.*, *ApJS*, **215**, 15, 2014.
10 H. A. Kobulnicky *et al.*, *ApJS*, **213**, 34, 2014.
11 D. M. Bowman *et al.*, *A&A*, **621**, A135, 2019.
12 J. Southworth & D. M. Bowman, *MNRAS*, **513**, 3191, 2022.
13 J. Southworth *et al.*, *MNRAS*, **497**, L19, 2020.
14 J. W. Lee & K. Hong, *AJ*, **161**, 32, 2021.
15 J. Southworth, D. M. Bowman & K. Pavlovski, *MNRAS*, **501**, L65, 2021.
16 F. Kahraman Aliçavuş *et al.*, *MNRAS*, **470**, 915, 2017.
17 X. Chen *et al.*, *ApJS*, **263**, 34, 2022.
18 J. Southworth, *The Observatory*, **141**, 282, 2021.
19 J. Southworth, S. J. Murphy & K. Pavlovski, *MNRAS*, **520**, L53, 2023.
20 J. Debosscher *et al.*, *A&A*, **556**, A56, 2013.
21 J. W. Lee, *ApJ*, **833**, 170, 2016.
22 J. Southworth & T. Van Reeth, *MNRAS*, **515**, 2755, 2022.
23 D. W. Kurtz *et al.*, *MNRAS*, **494**, 5118, 2020.
24 G. Handler *et al.*, *Nature Astronomy*, **4**, 684, 2020.
25 J. Southworth, *The Observatory*, **140**, 247, 2020.
26 J. Southworth, *Universe*, **7**, 369, 2021.
27 Gaia Collaboration, *A&A*, **649**, A1, 2021.
28 D. Hoffleit & C. . Jaschek, *The Bright Star Catalogue* (New Haven, Conn.: Yale University Observatory, 1991, 5th ed.), 1991.
29 A. J. Cannon & E. C. Pickering, *Annals of Harvard College Observatory*, **98**, 1, 1923.
30 K. G. Stassun *et al.*, *AJ*, **158**, 138, 2019.
31 E. Høg *et al.*, *A&A*, **355**, L27, 2000.
32 R. M. Cutri *et al.*, *2MASS All Sky Catalogue of Point Sources* (The IRSA 2MASS All-Sky Point Source Catalogue, NASA/IPAC Infrared Science Archive, Caltech, US), 2003.
33 W. W. Morgan & N. G. Roman, *ApJ*, **112**, 362, 1950.
34 J. S. Plaskett & J. A. Pearce, *PDAO*, **5**, 1, 1931.
35 P. Mayer & D. Chochol, *PASP*, **93**, 608, 1981.
36 J. R. Percy & D. L. Welch, *PASP*, **95**, 491, 1983.
37 W. W. Morgan, A. D. Code & A. E. Whitford, *ApJS*, **2**, 41, 1955.
38 W. A. Hiltner, *ApJS*, **2**, 389, 1956.
39 W. A. Hiltner, *ApJ*, **114**, 241, 1951.
40 J. R. Lesh, *ApJS*, **17**, 371, 1968.
41 G. Hill & W. A. Fisher, *A&A*, **139**, 123, 1984.
42 P. Mayer *et al.*, *BAICz*, **42**, 230, 1991.
43 T. Raja, *A&A*, **284**, 82, 1994.
44 D. M. Popper, *PASP*, **105**, 721, 1993.
45 J. R. Percy & N. Khaja, *JRASC*, **89**, 91, 1995.
46 G. J. J. Talens *et al.*, *A&A*, **601**, A11, 2017.

47 O. Burggraaff *et al.*, *A&A*, **617**, A32, 2018.
48 G. R. Ricker *et al.*, *Journal of Astronomical Telescopes, Instruments, and Systems*, **1**, 014003, 2015.
49 Lightkurve Collaboration, '(Lightkurve: Kepler and TESS time series analysis in Python)', Astrophysics Source Code Library, 2018.
50 J. M. Jenkins *et al.*, in *Proc. SPIE*, 2016, *Society of Photo-Optical Instrumentation Engineers (SPIE) Conference Series*, vol. 9913, p. 99133E.
51 J. Southworth, *The Observatory*, **142**, 267, 2022.
52 J. Southworth, P. F. L. Maxted & B. Smalley, *MNRAS*, **351**, 1277, 2004.
53 J. Southworth, *A&A*, **557**, A119, 2013.
54 H. N. Russell, *ApJ*, **36**, 54, 1912.
55 J. Southworth, *MNRAS*, **386**, 1644, 2008.
56 P. Lenz & M. Breger, in *The A-Star Puzzle, Cambridge University Press, Cambridge, UK.* (J. Zverko, J. Žižnovsky, S. J. Adelman, & W. W. Weiss, ed.), 2004, *IAU Symposium*, vol. 224, pp. 786–790.
57 D. M. Bowman *et al.*, *Nature Astronomy*, **3**, 760, 2019.
58 A. Tkachenko *et al.*, *MNRAS*, **438**, 3093, 2014.
59 T. M. Rogers *et al.*, *ApJ*, **772**, 21, 2013.
60 C. Aerts & T. M. Rogers, *ApJ*, **806**, L33, 2015.
61 S. Zucker & T. Mazeh, *ApJ*, **420**, 806, 1994.
62 S. Rucinski, in *IAU Colloq. 170: Precise Stellar Radial Velocities* (J. B. Hearnshaw & C. D. Scarfe, ed.), 1999, *Astronomical Society of the Pacific Conference Series*, vol. 185, p. 82.
63 K. P. Simon & E. Sturm, *A&A*, **281**, 286, 1994.
64 K. Pavlovski *et al.*, *MNRAS*, **400**, 791, 2009.
65 A. B. Underhill *et al.*, *MNRAS*, **189**, 601, 1979.
66 M. J. Pecaut & E. E. Mamajek, *ApJS*, **208**, 9, 2013.
67 Y. Wu *et al.*, *A&A*, **525**, A71, 2011.
68 A. Prša *et al.*, *AJ*, **152**, 41, 2016.
69 J. Southworth, P. F. L. Maxted & B. Smalley, *A&A*, **429**, 645, 2005.
70 L. Girardi *et al.*, *A&A*, **391**, 195, 2002.
71 G. Hill & A. H. Batten, *A&A*, **141**, 39, 1984.
72 D. M. Popper & E. F. Guinan, *PASP*, **110**, 572, 1998.
73 E. F. Guinan *et al.*, *ApJ*, **544**, 409, 2000.
74 A. Tkachenko *et al.*, *MNRAS*, **424**, L21, 2012.
75 W. J. Borucki, *Reports on Progress in Physics*, **79**, 036901, 2016.
76 Y. Chen *et al.*, *MNRAS*, **444**, 2525, 2014.